Reaction Kinetics, Mechanisms and Catalysis (2022) 135:1187–1209
https://doi.org/10.1007/s11144-022-02171-4

Identification of the best medium for experiments on chemical computation with Belousov–Zhabotinsky reaction and ferroin-loaded Dowex beads

F. Muzika[1] · **J. Górecki**[1]

Received: 16 November 2021 / Accepted: 20 January 2022 / Published online: 3 February 2022

Abstract

Our study is focused on identification of the best medium for future experiments on information processing with Belousov–Zhabotinsky reaction proceeding in Dowex beads with immobilized catalyst inside. The optimum medium should be characterized by long and stable nonlinear behavior, mechanical stability and should allow for control with electric potential. We considered different types of Dowex ion-exchange resins, bead distributions and various initial concentrations of substrates: malonic acid and 1,4-cyclohexanedione. The electric potential on platinum electrodes, stabilized by a potentiostat is used to control medium evolution. A negative electric potential generates activator species $HBrO_2$ on the working electrode according to the reaction: $BrO_3^- + 2e^- + 3H^+ \rightarrow HBrO_2 + H_2O$, while positive electric potential attracts inhibitor species Br^- to the proximity of it. We study oscillation amplitude and period stability in systems with ferroin loaded Dowex 50W-X2 and Dowex 50W-X8 beads during experiments exceeding 16 h. It has been observed, that the above mentioned resins generate a smaller number of CO_2 bubbles close to the beads than Dowex 50W-X4, which makes Dowex 50W-X2 and Dowex 50W-X8 more suitable for applications in chemical computing. We report amplitude stability, oscillation frequency, merging and annihilation of travelling waves in a lattice of Dowex 50W-X8 beads (mesh size 50–100) in over 19 h long experiments with equimolar solution of malonic acid and 1,4-cyclohexanedione. This system looks as a promising candidate for chemical computing devices that can operate for a day.

Keywords Belousov–Zhabotinsky · 1,4-Cyclohexanedione · Travelling wave · Polymer beads · Dowex · Electric potential

Abbreviations

MA Malonic acid

✉ F. Muzika
fmuzika@ichf.edu.pl

[1] Institute of Physical Chemistry Polish Academy of Sciences, Kasprzaka 44/52, 01-224 Warszaw, Poland

CHD	1,4-Cyclohexanedione
BZ	Belousov–Zhabotinsky
MA-BZ	Belousov–Zhabotinsky reaction using MA as the substrate
CHD-BZ	Belousov–Zhabotinsky reaction using CHD as the substrate
MA-CHD-BZ	Belousov–Zhabotinsky reaction using equimolar solution of MA and CHD as the substrates
TW	Travelling waves
GO	Global oscillations

Introduction

Unconventional computers, like chemical computing devices, are potential candidates to create an alternative to silicon-based microprocessors requiring large amount of energy to make them and to operate [1]. Interesting counterplay are liquid computers [2]. Even though they are several orders slower than modern silicon-based computers, they also offer multithreading and in the most of the cases neural network architecture. Liquid computers are not designed to work with the binary information coding, but yet they can effectively solve many problems, like for example the pattern recognition ones [3, 4]. Current silicon technology in cell phones also offers computing in neural processing units (NPUs) [5]. The information processing performed by liquid computers shows more similarities to that in living organisms than the computing done by semiconductor processors. Both liquid computers and living organisms need chemical energy to operate. They use non-electric inputs and CO_2 is one of waste products of information processing [6]. Nature-made liquid computers, like for example the Human brain, seem to be highly optimized for energy consumption. The brain performance is estimated around exaflop [7] while dissipating only 20 W of energy [8]. Such high performance/energy ratio in living organisms can only be achieved by combination of reaction–diffusion systems, neural network architecture and rapid electric impulses. Man-made liquid computers have already evolved from inorganic reaction networks into organic ones and their operation can be based on enzymes, RNA, DNA [9], enzymatic cascades [10–12] or protein structures [13]. However, a short lifetime of reactions responsible for information processing in liquid computers and the need to provide continuous inflow of chemical energy to support operations seem to be the major obstacles for prolonged operation.

The majority of liquid computers require a system of chemical reactions showing a nonlinear behaviour to operate. Probably the most studied set of reactions providing oscillations is the Belousov–Zhabotinsky reaction developed by [14] using citric acid and further modified by Zhabotinsky using malonic acid [15]. The reaction can proceed in a stirred tank reactor [16], gel discs [17], self-propelled gel system [18] or another planar oriented systems [19, 20]. To get closer to the cellular size and behavior, reactors are miniaturized into smaller sizes as microoscillators. There are currently three types of chemical microoscillators: polymeric microspheres with immobilized catalyst, which are later placed in a catalyst free BZ solution; BZ micro-droplets with all BZ

reagents inside and liposomes encapsulating the BZ reagents [21]. There have been many applications of Belousov–Zhabotinsky reaction for chemical computing [22].

BZ system using malonic acid (MA) as a substrate can supply liquid marble techniques for hours with stable oscillations, however it forms CO_2 as waste [23]. CO_2 bubbles are generated in between marbles or vesicles and disassemble the whole marble lattice. A similar problem appears in networks of droplets containing a solution of BZ-reagents, that are stabilized by phospholipids dissolved in the surrounding, organic phase [24]. This problem can be solved by using 1,4-cyclohexanedione (CHD) [25], however the lifetime of oscillations can be shorter [26]. Chang et al. showed that, the longer lifetime for BZ assemblages can be achieved by using equimolar solution of MA and CHD [23].

BZ reaction can be influenced by light [4, 27], sound [28], and electric potential [29, 30]. We are currently interested in the latest because the electrical interface using a potentiostat can switch between the regimes of travelling waves (TW) or global oscillations (GO) [30, 31]. Therefore, such system is interesting for chemical computing applications. Negatively polarized working electrode of potentiostat forms activator species $HBrO_2$, according to reaction: $BrO_3^- + 2e^- + 3H+ \rightarrow HBrO_2 + H_2O$ [29]. Positive electric potential on the working electrode attracts the inhibitor species Br^- from the solution near the working electrode. If Br^- is not added to the initial solution, it takes several hours to form it from brominated malonic acid [32] and brominated 1,4-cyclohexandedione [33].

The aim of this paper is to identify a variant of BZ-reaction proceeding in Dowex bead system can be useful for the future development of chemical computers. A number of recent theoretical papers [4, 34–36] is concerned with computing potential of networks formed by coupled chemical oscillators. In such network the input information is introduced by time dependent inhibition of oscillations. Output information can be extracted from a number of activator maxima observed on a selected node or from the frequency recorded on the output node [35]. The identification of an experimental system that exhibits oscillations with a stable period over a long time and a reliable method of oscillation control is crucial for practical realization of information processing networks. Having in mind nature-inspired geometry of information processing medium we investigated ion-exchange beads with the immobilized catalyst as candidates for network nodes. Such beads seem to form more stable networks than droplets containing reagents of BZ-reaction. Following [29, 30] we assumed that reaction proceeding in individual beads is controlled by the electric potential.

The "Experimental setup" section describes the reactor composition, beads, loading and image analysis. The "Experimental results" section describes and compares ion exchange resins Dowex 50W-X2/X4/X8, different concentration of reagents in the initial solutions and the presence of Br^- in the initial solution. The main results are summarized in Table 1 and in the "Discussion and conclusions" section.

Table 1 Summarized initial conditions of all experiments and electric potential effect on beads

Figures	Beads type (mesh size)	BZ reactants	MA or CHD	Electric potential (V)	Potenciostat control	Vol, ml	Resulting effect
Fig. 2c, d	X4 (20–50)	$[NaBrO_3]_0 = 0.2$ M $[H_2SO_4]_0 = 0.6$ M	$[MA]_0 = 0.4$	− 0.5	Global	3	Synchronization CO_2 bubbles
Fig. 2e, f	X4 (20–50)	$[NaBrO_3]_0 = 0.2$ M $[H_2SO_4]_0 = 0.6$ M	$[MA]_0 = 0.4$	+ 0.5	Global	3	Shorter periods if compared to − 0.5 V CO_2 bubbles
Fig. 3c, d	X2 (20–50) X8 (16–50)	$[NaBrO_3]_0 = 0.45$ M $[H_2SO_4]_0 = 0.9$ M	$[MA]_0 = 0.4$	− 1.5	Local + global	5	Long oscillation induction Oscillation desynchronization
Fig. 3e, f	X2 (20–50) X8 (16–50)	$[NaBrO_3]_0 = 0.45$ M $[H_2SO_4]_0 = 0.9$ M	$[MA]_0 = 0.4$	0.0	Local + global	5	Oscillation synchronization CO_2 bubbles
Fig. 4c, d	X4 (20–50)	$[NaBrO_3]_0 = 0.3$ M $[H_2SO_4]_0 = 0.6$ M	$[CHD]_0 = 0.4$	− 1.5	Global	3	Oscillation induction and oscillation death in 3.5 h
Fig. 4f, g	X4 (20–50)	$[NaBrO_3]_0 = 0.3$ M $[H_2SO_4]_0 = 0.6$ M $[NaBr]_0 = 0.066$ M	$[CHD]_0 = 0.4$	0.0	Global	3	Constant oscillations, until electric potential is applied
Fig. 5c, d	X4 (20–50)	$[NaBrO_3]_0 = 0.2$ M $[H_2SO_4]_0 = 0.6$ M,	$[CHD]_0 = 0.2$ $[MA]_0 = 0.2$	− 0.5	Global	3	Oscillation desynchronization
Fig. 5f, g	X4 (20–50)	$[NaBrO_3]_0 = 0.2$ M $[H_2SO_4]_0 = 0.9$ M	$[CHD]_0 = 0.2$ $[MA]_0 = 0.2$	− 0.5	Global	3	Oscillation self-induction Oscillation synchronization
Fig. 6	X8 (50–100)	$[NaBrO_3]_0 = 0.45$ M $[H_2SO_4]_0 = 0.9$ M	$[CHD]_0 = 0.2$ $[MA]_0 = 0.2$	− 0.5	Local	5	Oscillation synchronisation Wave merging into MMOs Wave annihilation
Fig. 7	X8 (50–100)	$[NaBrO_3]_0 = 0.45$ M $[H_2SO_4]_0 = 0.9$ M	$[CHD] = 0.2$ $[MA] = 0.2$	0.0	Local + global	5	Oscillation synchronisation Wave merging into MMOs Wave splitting from MMOs Wave annihilation

Experimental setup

Used chemicals: deionized water, ferroin solution 0.025 M from Sigma-Aldrich (Switzerland). $NaBrO_3$ 99% from Fluka (Netherlands). Sulfuric acid 95% from Chempur Poland, malonic acid (MA) 99% from Sigma-Aldrich (Japan), NaBr p.a. from Chempur Poland, 1,4-cyclohexanedione (CHD) 98% from Sigma-Aldrich (Germany), Acetone 99.5% from Avantor Performance Materials Poland S.A. Dowex 50W-X2/X4/X8 hydrogen form, highly acidic, with (50–100) mesh/20–50 mesh/(16–50) mesh + (50–100) mesh size from Sigma-Aldrich (USA). Specific BZ reaction mixture will be given for each shown experiment.

The supply solutions are prepared with high concentrations of reagents specifically: sulfuric acid (3 M), MA (1 M), CHD (1 M), $NaBrO_3$ (1.5 M), NaBr (1 M). These solutions are mixed together in proportions needed to get concentrations of reagents used in a given experiment.

Beads used in experiments are loaded with ferroin following the procedure described in Kuze et al. [37]. One gram of beads is poured in 10 ml of solution of ferroin and undergoes continuous stirring for 2 days. The 10 ml ferroin solution is created using 440 µl of 0.025 M solution of ferroin. After the stirring finishes, the beads with immobilized ferroin are used to make assemblages in BZ reactor. The change in solution color indicates that all ferroine is absorbed by the beads. The solution contains $440 \times 10^{-6}\ \mathrm{l} \times 0.025\ \mathrm{mol} \times \mathrm{l}^{-1} = 11 \times 10^{-6}$ mol of ferroin. 1 g of beads has a volume of 1 g/(1.04 g cm^{-3}) = 0.96 cm^3. Therefore, the concentration of ferroin in beads is 11×10^{-6} mol/0.96×10^{-3} l = 11.6×10^{-3} M. The average amount of ferroin per single bead in a particular Dowex type is calculated from the size distribution of beads measured for one gram of beads using ImageJ programme [38]. As an example of such estimation let us consider Dowex 50W-X8 with 16–50 mesh in which the average bead diameter is 0.80 mm. The average bead volume can be estimated as $(4/3) \times \pi \times (0.801/2)^3 \times 10^{-6}$ l = 0.269×10^{-6} l. The molar amount of ferroin per bead is then calculated as concentration of ferroin in beads multiplied as the average bead volume and we get 3.12×10^{-9} mol/bead. For the other types of Dowex resins used in experiments we obtained the following average diameters and ferroin loads:

- Dowex 50W-X2 (20–50 mesh): the average diameter 0.644 mm and 1.62×10^{-9} mol/bead,
- Dowex 50W-X4 (20–50 mesh): the average diameter 0.649 mm and 1.66×10^{-9} mol/bead,
- Dowex 50W-X8 (16–50 mesh): the average diameter 0.801 mm and 3.12×10^{-9} mol/bead,
- Dowex 50W-X8 (50–100 mesh): the average diameter 0.223 mm and 6.7×10^{-11} mol/bead.

Two types of platinum working electrodes are used, one of foil type and another of wire type. The foil type is used to create electric potential for observation of effect on ferroin loaded beads, which are not touching the electrode. We

can regard such type of medium control as the global one, influencing all beads in a similar way. The wire type is used to influence ferroin loaded beads, which are touching the electrode. Such type of control is a local one and the perturbation can expand in the medium via bead-to-bead interactions. The wire electrode can provide input signal for future chemical computing applications.

The experimental setup is shown in Fig. 1. The ambient temperature is maintained at 23 ± 1 °C. There are three types of reactors, marked with **1** in Fig. 1a–c. They have different volumes. The reaction mixture volume, is either 5 ml or 3 ml. At the beginning of an experiment, the working electrode (WE) **3** of a potentiostat **5** is placed inside reactor **1**. Counter electrode (CE) and reference electrode (RE) are connected to one platinum electrode **4**, which is placed on the reactor wall. The reactor **1** is then filled with BZ solution and the ferroin loaded Dowex beads **2** are placed inside. The dynamic regimes of reduced and oxidized ferroin are then recorded by camera **6** with a magnification lens **7**. The electric potential inside the system is controlled using potentiostat **5**. After the experiment both reactor and electrodes are washed by acetone [23].

Imaging and analysis

The time evolution of the beads is recorded using Sony camera FDR-AX53 using MTS format. The native camera zoom is enhanced by additional macro lenses with magnifications 110× and 140× attached to the camera lens with a custom-made aluminium tube. The resolution is set to 1440×1080, and the recording rate is 25 fps what makes the overall data transfer rate 9 MB/s AVCHD. Videos are re-encoded without quality loss using the ffmpeg program. The resulting videos are cut and reformatted to 1920×1080 resolution into a single JPEG file per frame of video.

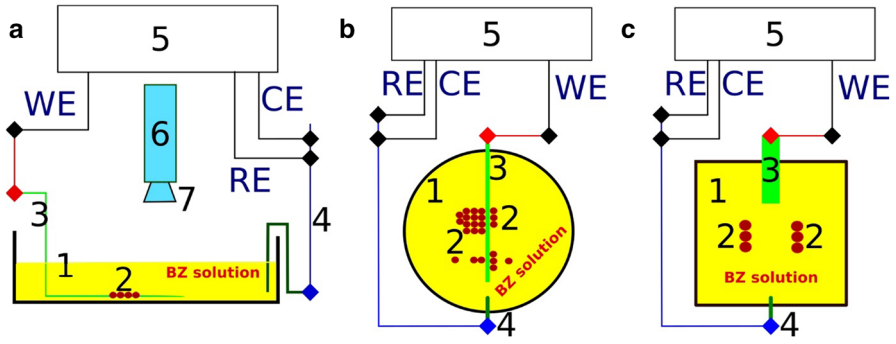

Fig. 1 Experimental setup **a** side view, **b** top view for platinum wire electrode setup, **c** top view for platinum foil electrode setup. WE represents working electrode of the potentiostat, CE represents counter electrode of the potentiostat and RE represents reference electrode of the potentiostat. (1a) batch reactor with BZ solution, (1b) glass tank batch reactor with diameter 3 5 mm and depth 7.3 mm filled with 5 ml BZ solution, (1c) polymeric tank batch reactor with two respective sizes and volumes: 36.4 mm × 36.4 mm × 6.2 mm filled with 5 ml BZ solution and 20.8 mm × 31.2 mm × 3.1 mm filled with 3 ml BZ solution; (2) ferroin loaded Dowex beads; (3a) platinum working electrode, (3b) platinum wire working electrode, (3c) platinum foil working electrode; (4) platinum electrode RE + CE, (5) potentiostat WIN13; (6) camera; (7) magnifying lenses ×140–×110

The resolution change is done to maintain the aspect ratio 16:9 because AVCHD uses non-square pixels. Stacks of JPEG files are loaded using ImageJ program [38]. Each bead is marked, and cross-sections through the stack of pictures are made to reduce the dimensionality into one spatial dimension and time. The sequence of cross-sections in time is combined together to create a space–time plot. The whole space–time plot is next split into color channels red, green, and blue. The green channel shows the highest contrast between oxidized and reduced states of ferroin and it is used for further analysis. One point from a slice of each bead (blue in figures) is chosen to show green channel baseline corrected intensity as a function of time. This function is then analyzed for the maxima and periods of oscillations using a custom written procedure.

Experiments

The experimental runs are from 7 to 19 h. Each experiment is performed for a fixed spatial distribution of ferroin loaded beads and the geometry of electrodes. During each experiment the working electrode potential changes in time in a piecewise form where every piece represents a constant value. Therefore, an experiment can be divided into time subintervals within which the electrode potential is constant. In Figs. 2, 3, 4, 5, 6 and 7 we show the time evolution of excitations observed on beads for different solutions of BZ-reagents, different types and diameters of beads, different types of electrodes and for different geometries of bead networks. The initial conditions of experiments discussed in this Section and the effects of applied electric potential are summarized in Table 1.

The first experimental system with MA-BZ is designed to investigate the influence of global control on groups of three and four beads. The system is illustrated in Fig. 2; it uses seven ferroin loaded Dowex 50W-X4 beads with mesh size 20–50. The experiment is performed in a plastic reactor and the beads are located in the cut trenches. This system has been divided into two groups of beads (see Fig. 2a). Four beads are in a row on the left side of the reactor and three beads in a row on the right side of the reactor. None of them touches the platinum foil electrode. The working electrode between the rows is set for global control. The bead-crossing green lines with a blue dot indicate where the illumination intensity data (the green components of pixels) for the corresponding space–time plots (cf. Fig. 2c) has been measured. Each of the blue lines in Fig. 2d represents the green component of the pixels located at the corresponding blue-marked dot as a function of time. This quantity is the basic result of experiment analysis. In the following we use the term "period" to describe the time between successive maxima of the green component in the considered time interval. The green component reflects the time dependence of concentration of oxidized ferroin at the point of observation. The same description of experimental setup and presentation of results is used in Figs. 3, 4, 5, 6 and 7.

In the experiment shown in Fig. 2 the volume of reagents is 3 ml and the initial concentrations in reaction mixture are $[NaBrO_3]_0 = 0.2$ M, $[MA]_0 = 0.4$ M, $[H_2SO_4]_0 = 0.6$ M. The initial concentrations of $NaBrO_3$ and MA are the same as in the work by Kuze et al. [29], but we use lower initial concentration of sulfuric acid.

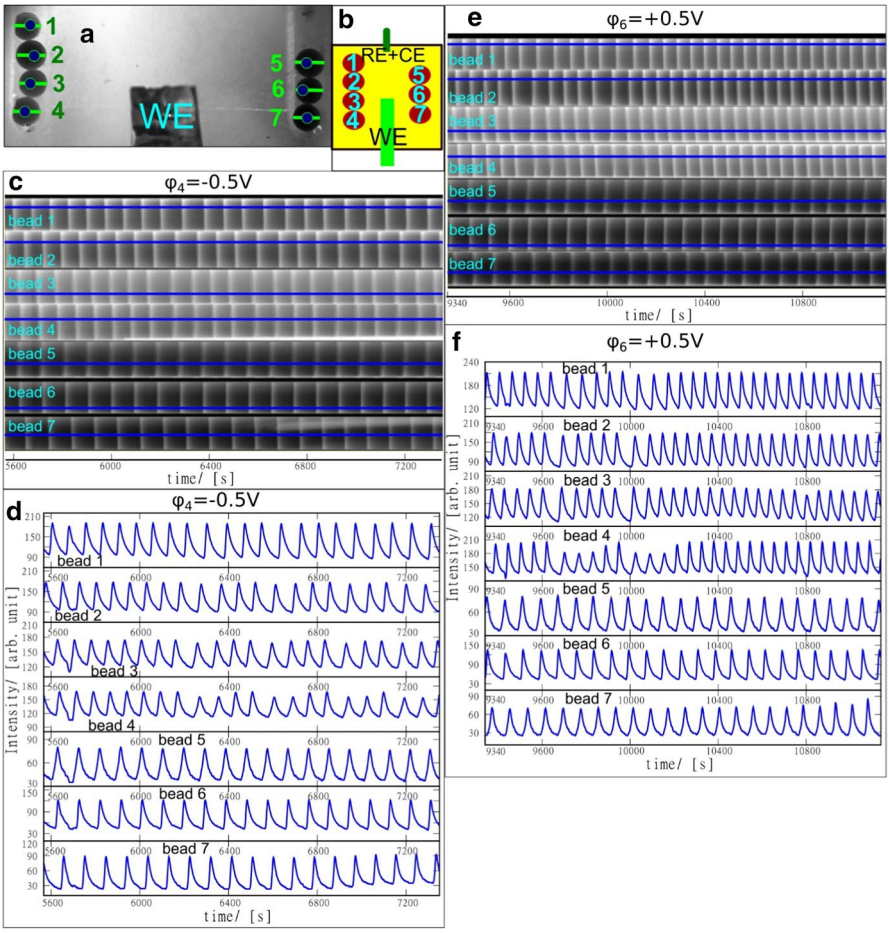

Fig. 2 Time evolution of MA-BZ system with platinum foil 3.1 mm wide as a working electrode and Dowex 50W-X4 beads with the mesh size 20–50 used for ferroin immobilization. The volume of reagents is 3 ml and the initial concentrations are $[NaBrO_3]_0 = 0.2$ M, $[MA]_0 = 0.4$ M, $[H_2SO_4]_0 = 0.6$ M. In this system we compare the influence of applied electric potential on the period of oscillations inside the ferroin loaded Dowex beads. The values of applied electric potential are: $\varphi_1 = 0.0$ V for times from 0 to 1975s, $\varphi_2 = -1.5$ V for times from 1975 to 3832 s, $\varphi_3 = -1.0$ V for times from 3832 to 5567 s, $\varphi_4 = -0.5$ V for times from 5567 to 7424 s, $\varphi_5 = 0.0$ V for times from 7424 to 9340 s and $\varphi_6 = +0.5$ V for times from 9340 to 11,140 s. **a** The enhanced contrast picture of the assemblage with numbered beads. The green lines mark cross sections for the space–time plots illustrated in (**c, e**). The blue dots show locations of points at which the intensity of the green component was measured (c.f. (**d, f**)). WE marks the working electrode. **b** The schematic diagram of the assemblage with numbered beads, RE + CE—reference and counter electrode; **c** the space–time plots of the green component intensity for all seven beads in the time interval [5567 s, 7350 s] in which the applied potential is $\varphi_4 = -0.5$ V. The green component intensities are measured along the green lines; **d** the green component intensities observed on all beads as functions of time in the time interval [5567 s, 7350 s], **e** the space–time plots of the green component intensity for all seven beads in the time interval [9340 s, 11,140 s] in which the applied potential is $\varphi_6 = +0.5$ V, **f** the green component intensities observed on all beads as functions of time in the time interval [9340 s, 11,140 s]. (Color figure online)

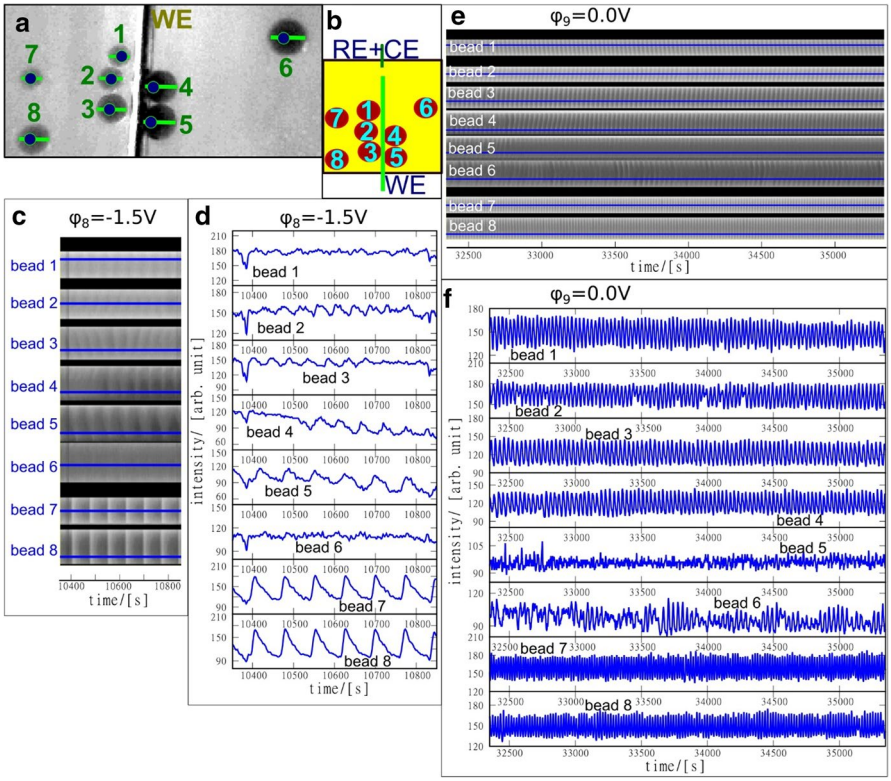

Fig. 3 Time evolution of MA-BZ system with platinum wire 0.43 mm in diameter as a working electrode and the mixture of Dowex 50W-X2 beads with mesh size 20–50 and Dowex 50W-X8 beads with mesh size 16–50 used for ferroin immobilization. The volume of reagents is 5 ml and the initial concentrations are: $[NaBrO_3]_0 = 0.45$ M, $[MA]_0 = 0.4$ M, $[H_2SO_4]_0 = 0.9$ M. In this system we compare influence of applied electric potential on periods of oscillations inside the ferroin loaded Dowex beads. The values of applied electric potential are: $\varphi_1 = 0.0$ V for times from 0 to 1915s, $\varphi_2 = -1.5$ V for times from 1915 to 2455 s, $\varphi_3 = 0.0$ V for times from 2455 to 3055 s, $\varphi_4 = -1.5$ V for times from 3055 to 6043 s, $\varphi_5 = 0.0$ V for times from 6043 to 7897 s, $\varphi_6 = -1.5$ V for times from 7897 to 8857 s, $\varphi_7 = 0.0$ V for times from 8857 to 10,351 s, $\varphi_8 = -1.5$ V for times from 10,351 to 10,886 s, and $\varphi_9 = 0.0$ V for times from 10,886 to 69,228 s. **a** The assemblage with numbered beads; beads No. 1–3 are Dowex 50W-X2, beads No. 4–8 are Dowex 50W-X8. The meanings of green lines and blue dots in (**a**) are the same as in Fig. 2. **b** the schematic diagram of the assemblage with numbered beads. **c** The space–time plots of the green component intensity for all beads in the time interval [10,351 s, 10,850 s] in which the applied potential is $\varphi_8 = -0.5$ V. **d** The green component intensities observed on all beads as functions of time in the time interval [10,351 s, 10,850 s]. **e** The space–time plots of the green component intensity for all beads in the time interval [32,350 s, 35,350 s] in which the applied potential is $\varphi_9 = 0.0$ V. **f** The green component intensities observed on all beads as functions of time in the time interval [32,350 s, 35,350 s]. (Color figure online)

All beads start oscillating immediately after placing them inside the reactor with the period of 30 ± 5 s. However, after a few minutes, the group of three beads (No. 5–7) changes its period to 150 ± 5 s, while the group of four beads (No. 1–4) switch into 170 ± 5 s period after 20 min. This occurs under $\varphi_1 = 0.0$ V. When electric potential

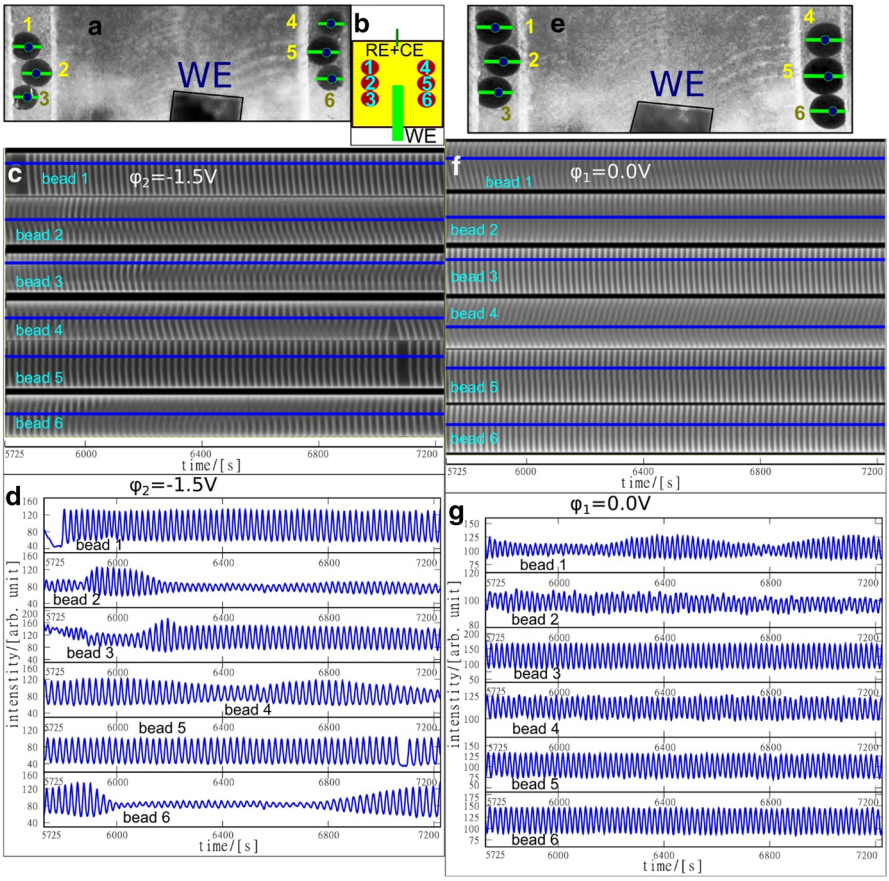

Fig. 4 Time evolution of two CHD-BZ system with platinum foil 3.1 mm wide as a working electrode and Dowex 50W-X4 beads with mesh size 20–50 used for ferroin immobilization. The volume of reagents is 3 ml. In these experiments we compare the evolution of a system without Br^- (**a**) in the initial solution with $\varphi_2 = -1.5$ V with system with Br^- (**e**) in the initial solution together with $\varphi_1 = 0.0$ V. The initial concentrations are: $[NaBrO_3]_0 = 0.3$ M, $[CHD]_0 = 0.4$ M, $[H_2SO_4]_0 = 0.6$ M for the solution without Br^- (**c, d**) and $[NaBrO_3]_0 = 0.3$ M, $[NaBr]_0 = 0.066$ M, $[CHD]_0 = 0.4$ M, $[H_2SO_4]_0 = 0.6$ M for the solution with Br^- ions (**f, g**). The values of applied electric potential applicable for system without Br^- in the initial solution (**c, d**) are: $\varphi_1 = 0.0$ V for times from 0 to 2212 s and $\varphi_2 = -1.5$ V for times from 2212 to 14,900 s. For system with Br^- ions present in the initial solution (**e, f**) the electric potential $\varphi_1 = 0.0$ V during the whole experiment (from 0 to 10,440 s). The green lines mark cross sections for the space–time plots illustrated in (**c, f**) and the blue dots show locations of points at which the intensity of the green component shown in (**d, g**) is measured. **b** The schematic diagram of the assemblage with numbered beads. **c, f** The space–time plots of the green component intensity for all beads in the time interval [5725 s, 7225 s]; for **c** the applied potential is $\varphi_2 = -1.5$ V and for **f** the applied potential is $\varphi_1 = 0.0$ V. **d, g** The green component intensities observed on all beads at as functions of time in the time interval [5725 s, 7225 s]; for **d** the applied potential is $\varphi_2 = -1.5$ V and for **g** the applied potential is $\varphi_1 = 0$ V. (Color figure online)

is changed $\varphi_2 = -1.5$ V, the period gradually decreases to 90 ± 4 s for the group of four beads (No. 1–4) and to 110 ± 4 s for the group of three beads (No. 5–7). The

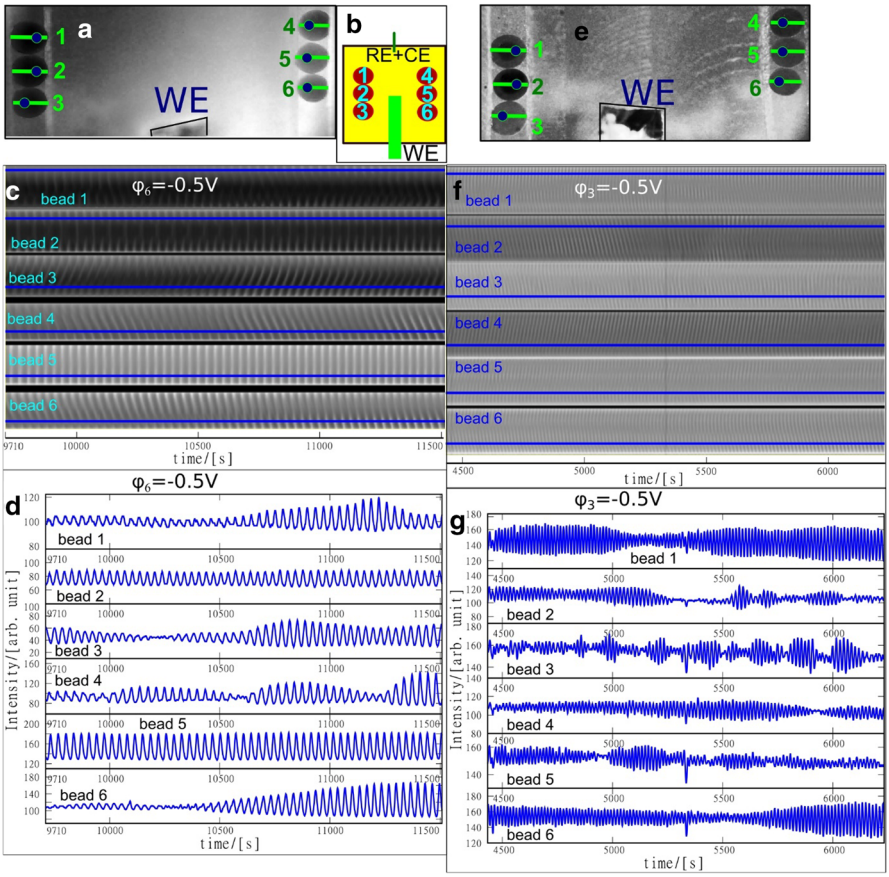

Fig. 5 Time evolution of MA-CHD-BZ systems with platinum foil 3.1 mm wide as a working electrode and the Dowex 50W-X4 beads with mesh size 20–50 used for ferroin immobilization. The volume of reagent mixture is 3 ml. The initial concentrations for system (**a**) and **c, d** are: $[NaBrO_3]_0 = 0.2$ M, $[MA]_0 = 0.2$ M, $[CHD]_0 = 0.2$ M, $[H_2SO_4]_0 = 0.6$ M. The initial concentrations for system (**e**) and **f, g** are: $[NaBrO_3]_0 = 0.2$ M, $[MA]_0 = 0.2$ M, $[CHD]_0 = 0.2$ M, $[H_2SO_4]_0 = 0.9$ M. In these systems we compare influence of initial concentration of sulfuric acid on periods of oscillations inside the ferroin loaded Dowex beads while the applied electric potential and the length of observation (1800 s) are the same. The values of applied electric potential for the system **a** are: $\varphi_1 = 0.0$ V for times from 0 to 1856 s and $\varphi_2 = +1.5$ V for times from 1856 to 4253 s, $\varphi_3 = +1.0$ V for times from 4253 to 6171 s, $\varphi_4 = +0.5$ V for times from 6171 to 7850 s, $\varphi_5 = 0.0$ V for times from 7850 to 9709 s and $\varphi_6 = -0.5$ V for times from 9709 to 11,567 s. The values of applied electric potential for the system **e** are: $\varphi_1 = 0.0$ V for times from 0 to 2396 s and $\varphi_2 = +0.5$ V for times from 2396 to 4433 s, $\varphi_3 = -0.5$ V for times from 4433 to 10,685 s. The meanings of green lines and blue dots in (**a**) are the same as in Figure. **b** The schematic diagram of the assemblage with numbered beads. **c** The space–time plots of the green component intensity for all beads in the time interval [9709 s, 11,509 s] in which the applied potential is $\varphi_6 = -0.5$ V. **d** The green component intensities observed on all beads as functions of time in the time interval [9709 s, 11,509 s]. **f** The space–time plots of the green component intensity for all beads in the time interval [4433 s, 6233 s] in which the applied potential is $\varphi_3 = -0.5$ V. **g** the green component intensities observed on all beads as functions of time in the time interval [4433 s, 6233 s]. (Color figure online)

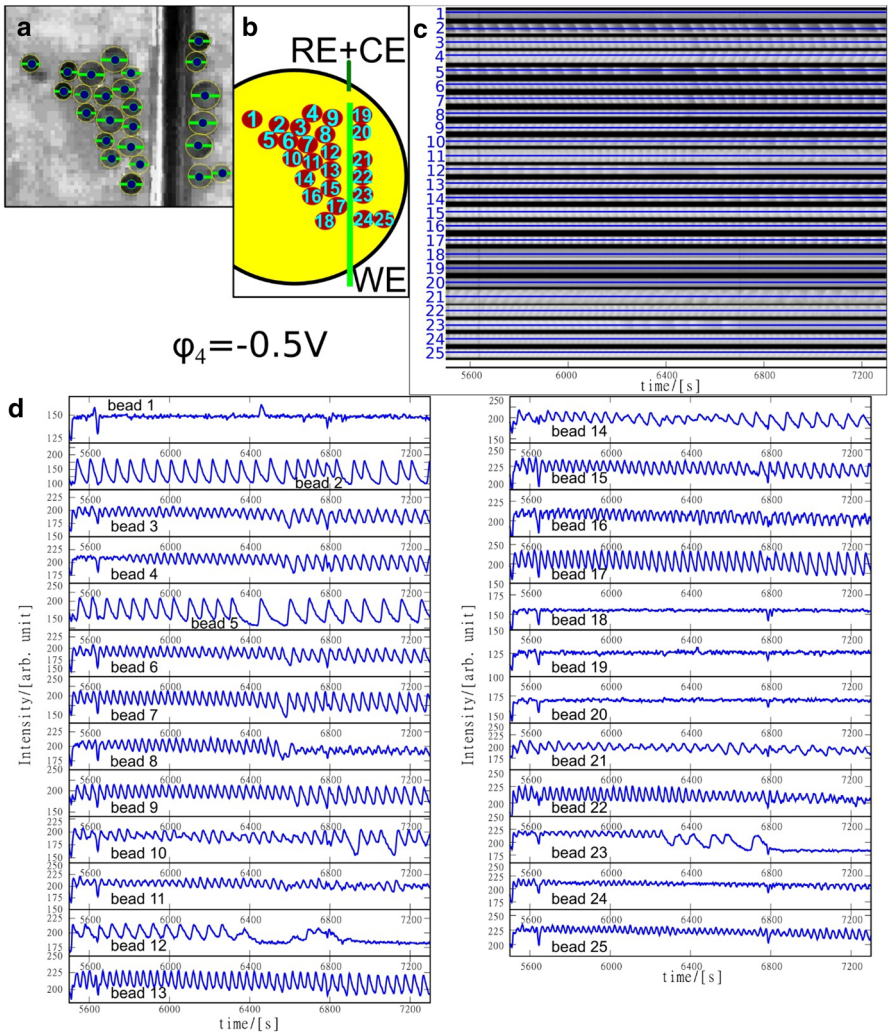

Fig. 6 Time evolution of MA-CHD-BZ system with platinum wire 0.43 mm in diameter as a working electrode and the mixture of Dowex 50W-X8 beads with mesh size 50–100 used for ferroin immobilization. The volume of reagents is 5 ml and the initial concentrations are: $[NaBrO_3]_0 = 0.45$ M, $[MA]_0 = 0.2$ M, $[CHD]_0 = 0.2$ M, $[H_2SO_4]_0 = 0.9$ M. The values of applied electric potential are: $\varphi_1 = 0.0$ V for times from 0 to 1791s, $\varphi_2 = -0.5$ V for times from 1791 to 3705 s, $\varphi_3 = +0.5$ V for times from 3705 to 5496 s, $\varphi_4 = -0.5$ V for times from 5496 to 7350 s, $\varphi_5 = +0.5$ V for times from 7350 to 9086 s, $\varphi_6 = -0.5$ V for times from 9086 to 11,061 s, $\varphi_7 = +0.5$ V for times from 11,061 s to 12,676 s, $\varphi_8 =$ -0.5 V for times from 12,676 to 14,605 s, $\varphi_9 = +0.5$ V for times from 14,605 to 16,565 s, $\varphi_{10} = -0.5$ V for times from 16,565 to 18,362 s, $\varphi_{11} = +0.5$ V for times from 18,362 to 19,806 s, $\varphi_{12} = -0.5$ V for times from 19,806 to 22,074 s, $\varphi_{13} = +0.5$ V for times from 22,074 to 23,507 s, $\varphi_{14} = -1.5$ V for times from 23,507 to 25,243 s, $\varphi_{15} = 0.0$ V for times from 25,243 to 72,123 s. **a** The assemblage with numbered beads. The meanings of green lines and blue dots in (**a**) are the same as in Fig. 2. **b** the schematic diagram of the assemblage with numbered beads. **c** The space–time plots of the green component intensity for all beads (beads are marked by blue numbers only) in the time interval [5500 s, 7300 s] in which the applied potential is $\varphi_4 = -0.5$ V. **d** The green component intensities observed on all beads as functions of time in the time interval [5500 s, 7300 s]. (Color figure online)

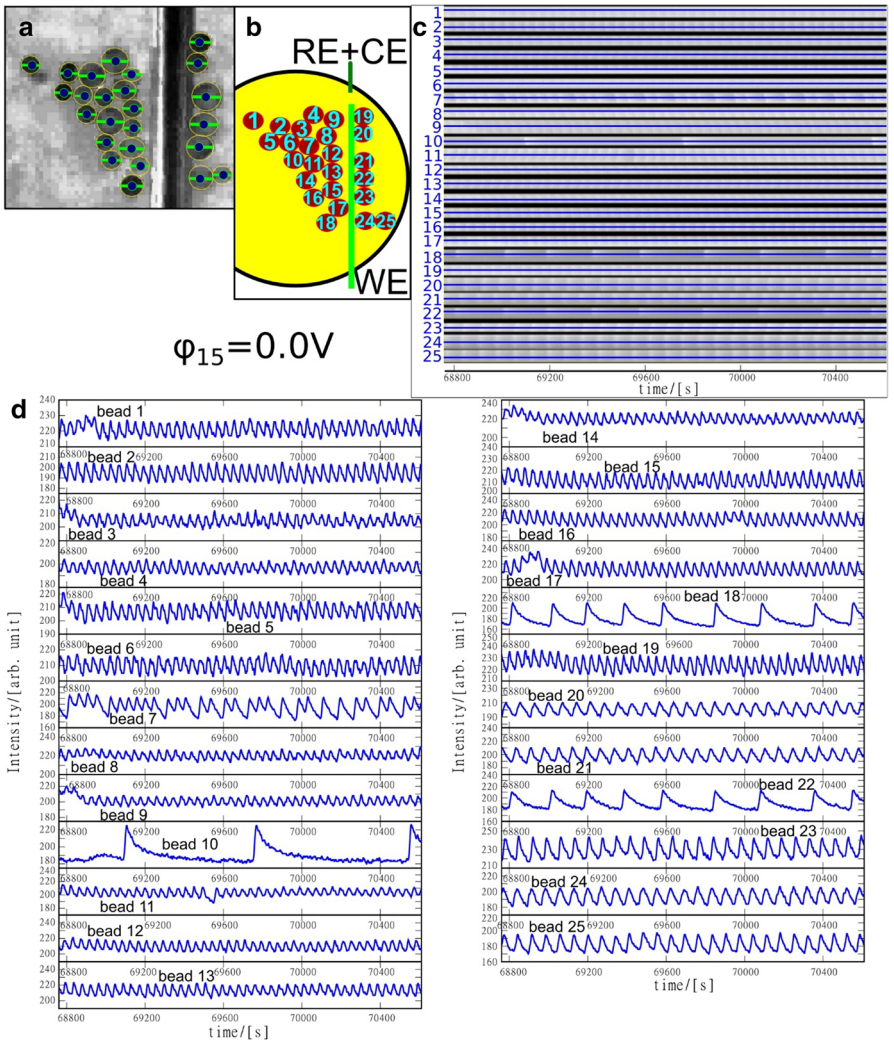

Fig. 7 The long-time evolution of MA-CHD-BZ system illustrated in Fig. 6. **a** The snapshot showing location of beads (cf. Fig, 6a). **b** The schematic diagram of the assemblage with numbered beads. **c** The space–time plots of the green component intensity for all beads (beads are marked by blue numbers only) in the time interval [68,760 s, 70,610 s] in which the applied potential is $\varphi_{15}=0.0$ V. **d** The green component intensities observed on all beads as functions of time in the time interval [68,760 s, 70,610 s]. (Color figure online)

change into third electric potential step $\varphi_3=$ - -1.0 V decreases slowly the period in the group of four beads (No. 1–4) to 80 ± 3 and for the group of three beads (No. 5–7) to 96 ± 3 s. The effect of the fourth electric potential step $\varphi_4=-0.5$ V forced in time interval [5567 s, 7350 s] are shown in Fig. 2c, d). This phase of experiment seems interesting because it demonstrates potential-induced synchronization of periods at the end of the presented time interval. The period of the group of four

beads (No. 1–4) starts at 75 ± 2 s and slowly increases to 90 ± 2 s at the end of this experimental phase. The period of the group of three beads (No. 5–7) shows opposite but continuous trend. At the beginning of the considered time interval, it is 95 ± 1 s and it slowly decreases to 90 ± 1 s at the end of this experimental phase. At the beginning of next potential step $\varphi_5 = 0.0$ V all beads are oscillating with the period 90 ± 3 s. Next, the period in the group of four beads (No. 1–4) decreases during this experimental phase to 80 ± 2 s, while the period in the group of three beads (No. 5–7) remains stable at 87 ± 3 s. The effects observed at the next potential step $\varphi_6 = +0.5$ V for the time interval [9340 s, 11,140 s] are shown in Fig. 2e and f. We selected this experimental phase to show the influence of electric potential under global control. The period of the group of four beads (No. 1–4) switches into regime 55 ± 3 s, while the period in the group of three beads (No. 5–7) slowly decreases from 87 ± 3 to 72 ± 2 s. When we compare groups of three and four ferroin loaded Dowex 50W-X4 type beads with global control, the group of four beads show shorter period than group of three beads when zero electric potential is applied. We can conclude that in the long-time experiments, the global control with negative electric potential results in synchronization of period regardless of numbers of beads in the group. On the other hand, the global control using a positive electric potential makes the period of oscillations shorter, but the effect becomes more important for larger number of beads in the group. The formation of CO_2 bubbles can also be observed in Fig. 2a) near bead No. 4 and bead No. 7. This is most likely caused by accumulation of Br_2 in the trenches in the reactor after a previous experiment, because the edges of trenches are hard to wash by acetone [23].

The second experimental system, shown in Fig. 3, illustrates a long-time stability of the amplitude of oscillations in MA-BZ reaction and the influence of the electrode that introduces both local and global control. This experiment is performed with initial concentrations $[NaBrO_3]_0 = 0.45$ M, $[MA]_0 = 0.4$ M, $[H_2SO_4]_0 = 0.9$ M, which is higher in $NaBrO_3$ and H_2SO_4 compared to experiment shown in Fig. 2. In this experiment we use a platinum wire electrode and a mixture of 8 beads, numbered as indicated in Fig. 3b. Considering the location of working electrode as the reference line of the picture, three beads touching the electrode from the left are made of Dowex 50W-X2 with mesh size 20–50 (No.1, 2, 3). The two separate beads to the left (No. 7, 8) and all beads on the right (No. 4, 5, 6) are Dowex 50W-X8 with mesh size 16–50. First three electric potential steps $\varphi_1 = 0.0$ V, $\varphi_2 = -1.5$ V, $\varphi_3 = 0.0$ V do not induce oscillations inside any ferroin loaded Dowex beads in this experiment. The fourth potential step $\varphi_4 = -1.5$ V induces oscillations with 30 ± 2 s period in the bead No.7 and with 20 ± 3 s period in the bead No. 8. Both beads keep oscillating even under $\varphi_5 = 0.0$ V but with period 90 ± 5 s for the bead No. 7 and 83 ± 2 s for the bead No. 8. When sixth electric potential step $\varphi_6 = -1.5$ V is applied, it induces oscillation in beads No. 1–3 with bead dependent period from 35 to 50 s and it decreases slightly the period in the bead No. 7 to 87 ± 2 s and in the bead No. 8 to 78 ± 3 s. The seventh electric potential step $\varphi_7 = 0.0$ V introduces synchronization of oscillations in beads No. 1–3 at 44 ± 7 s period and the periods of beads No. 7 and No. 8 are slowly decreased to 76 ± 1 s. The results of next electric potential step $\varphi_8 = -1.5$ V are shown in Fig. 3c and d for the time interval [10,351 s, 10,850 s]. At this stage oscillations in beads No. 4 and No. 5 are introduced by the local

control. Desynchronization of period occurs in beads No. 1–3 to 55 ± 5 s, 30 ± 5 s and 45 ± 5 s. The period in bead No. 4 is 48 ± 5 s and in bead No. 5 it is 62 ± 11 s. The periods in beads No. 7 and No. 8 decreases to 73 ± 2 s. In Fig. 3e and f, we present the results for the time interval [32,350 s, 35,350 s] which corresponds to the electrode potential $\varphi_9 = 0.0$ V. We select this particular interval to show stability of oscillations even after a long time of the experiment. The meanings of green lines and blue dots are the same as in Fig. 2. Around the time t = 10,886 s the oscillations of beads No. 1–3 are unsynchronized and their periods are in the range between 60–80 s. At the time around t = 22,800 s the periods synchronize at 30 ± 2 s. The beads oscillate with such period till the end of the experiment at t = 69,228 s. We observed that the initial period of beads No. 4 and No. 5 in the 9th potential phase are 50 ± 2 s, then they increase to 80 s and finally decrease to 25 ± 2 s at around t = 22,800 s. The beads No. 6 and No. 7 start to oscillate with period synchronized at 50 ± 5 s, then it increases and decreases by up to 20 s. At t = 22,800 s, they synchronize at 30 ± 2 s. The oscillations of the standalone bead No. 8 start with the period of 73 s, it slowly decreases to 30 ± 2 s at t = 22,800 s. The above mentioned periods of oscillations in beads 4–8 remain stable after t = 22,800 s for another 13 h. We also observed, that at these experimental conditions the geometry of beads is not stable; the beads No. 1 and No. 2 are shifted away by CO_2 bubble during the 16 h long experimental phase under $\varphi_9 = 0.0$ V. This experiment shows that synchronization and desynchronization of oscillations in a group of beads can be forced by application of electric potential and it appears when neutral and negative electric potentials are applied respectively. We also observed that oscillations can be induced inside ferroin loaded Dowex 50W-X8 with global control. When oscillation induction by global control occurs, the periods are not controllable by negative electric potential change. Oscillations inside ferroin loaded Dowex 50W-X8 can also be induced by local control using a negative electric potential. The local control can be also used to control periods inside ferroin loaded Dowex 50W-X8. These features make Dowex 50w-×8 beads promising candidates for chemical computing devices. On the other hand, oscillations inside ferroin loaded Dowex 50W-X2 under local control seem to be developed in time regardless of applied negative electric potential. The desynchronization under zero electric potential for the long-time experiment is caused by interactions of TWs inside the bead lattice due to random spatial distribution of this lattice.

In the next reported experiment (Fig. 4) we studied the CHD-BZ reaction which is a bubble-free variant of BZ-reaction. We expected to identify a medium that is not mechanically disturbed by the gas release. The goal of this experiment is to compare the time evolution of similar geometry of ferroine loaded beads in a system without Br^- ions in the initial mixture of reagents and a system where Br^- ions are introduced in the initial mixture of reagents. As the system with no Br^- ions in the initial reaction mixture we considered the following concentrations of reagents: $[NaBrO_3]_0 = 0.3$ M, $[CHD]_0 = 0.4$ M, $[H_2SO_4]_0 = 0.6$ M together with application of electric potential via global control. As the medium with Br^- ions we considered $[NaBrO_3]_0 = 0.3$ M, $[NaBr]_0 = 0.066$ M, $[CHD]_0 = 0.4$ M, and $[H_2SO_4]_0 = 0.6$ M. For this system the electrode potential is $\varphi_1 = 0.0$ V during the whole experiment. The value of $[H_2SO_4]_0$ is the same as in the experiment shown in Fig. 2 and $[CHD]_0$ has

the same initial concentrations as MA in both Figs. 2 and 3. The difference between this and the previous experiments is in the increased initial concentration of $NaBrO_3$ and in addition of NaBr in one of the systems. Dowex 50W-X4 beads with mesh size 20–50 are used for ferroin immobilization for both experiments. The experimental layout of the system without Br^- is shown in Fig. 4a and the experimental layout of the system with Br^- is shown in Fig. 4e. Beads are assembled in two rows three pieces each in trenches as indicated in Fig. 4a, b and e. The green lines mark cross sections for the space–time plots illustrated in (c, f) and the blue dots show locations of points at which the intensity of the green component shown in (d, g) is measured. At the initial stage of experiment without Br^- ions in the initial reaction mixture, when the applied potential is $\varphi = 0.0$ V we do not observe oscillations on beads. Fig. 4c and d illustrate space–time plots of the green component intensity for all beads and the green component intensities observed on all beads at the blue points as functions of time in the interval [5725 s, 7225 s] for the mixture without Br^- ions at the beginning of experiment. In this time interval the applied potential is $\varphi_2 = -1.5$ V. All beads show the period of 23 ± 2. However, the oscillation amplitudes are not constant because in beads No. 2 and No. 6 the observation points are in the area where TW are merging. The system without Br^- in initial reagents and negative electric potential has an oscillation lifetime of 3.5 h. However, oscillations do not occur spontaneously when no electric potential is applied. The period of CHD-BZ oscillations initiated by a negative electric potential is short just after they appear (around 11 s) and gradually increases to 40–50 s before the oscillations stop. This is the effect of global control. Negative electric potential generates activator, but also repulses inhibitor, Br^-, which slowly cumulates for 3.5 h and kills oscillations inside the beads. Fig. 4d and g present the same functions in the time interval [5725 s, 7225 s] for the mixture with Br^- ions. We chose this time interval to illustrate that periods in both systems are similar (20 ± 2 s). Only the bead No. 1 shows amplitude instability, also caused by wave merging. This can be seen from Fig. 4d, where the bead No.1 has wavy TWs, while the rest of the beads have TW more or less straight in shape. The period remains stable during the whole experimental time if zero electric potential is hold. The application of positive electric potential stops the oscillations.

Following the work by Chang et al. [23], we considered different compositions of MA and CHD to get rid of most of the CO_2 bubbles using CHD and prolong the lifetime of oscillation above 3.5 h using MA. Our experiments confirmed results of Chang and collaborators, that the equimolar mixture of MA and CHD has the required properties. The time evolution of MA-CHD-BZ systems with platinum foil 3.1 mm wide working electrode and the Dowex 50W-X4 beads with mesh size 20–50 used for ferroin immobilization is presented in Fig. 5. Two initial concentrations of medium are used: $[NaBrO_3]_0 = 0.2$ M, $[CHD]_0 = 0.2$ M, $[H_2SO_4]_0 = 0.6$ M (cf. Fig. 5a) and $[NaBrO_3]_0 = 0.2$ M, $[CHD]_0 = 0.2$ M, $[H_2SO_4]_0 = 0.9$ M (cf. Fig. 5e). Both systems were investigated under the same electric potential and global control, but they differ in the value of initial concentration of H_2SO_4. We selected the above concentrations to study the importance of $[H_2SO_4]_0$ for initiation of oscillations. The volume of reagent mixture is 3 ml. The initial concentration of $NaBrO_3$ matches the initial concentrations in Fig. 2 and the equimolar initial concentrations

of MA and CHD sums up to initial concentrations of pure MA in Figs. 2 and 3 or initial concentration of pure CHD in Fig. 4. The oscillations inside beads are initiated by $\varphi_2 = +1.5$ V in the system (Fig. 5a) with the period around 30 ± 2 s. When electric potential is changed to $\varphi_3 = +1.0$ V, a lot of wave merging is observed in all beads making the period between 30 and 38 s. The fourth electric potential step $\varphi_4 = +0.5$ V produces more stable period of travelling waves at 35 ± 2 s in beads No. 3–6 and 30 ± 2 s for beads No. 1 and No. 2. The fifth electric potential step $\varphi_5 = 0.0$ V stabilizes the period around 33 ± 2 s and wave merging is apparent especially in bead No. 1 and No. 2. The green lines in Fig. 5a mark cross sections for the space–time plots illustrated in Fig. 5c and the blue dots show locations of points at which the intensity of the green component shown in Fig. 5d is measured. Fig. 5c and d show the results obtained in the time interval [9709 s, 11,509 s] in which the applied potential is $\varphi_6 = -0.5$ V. This time interval has been chosen to show desynchronization of oscillations in a bead lattice. The green component intensities (cf. Fig. 5d) strongly depend on time, showing intensive wave merging. At the beginning of the considered time interval periods in all beads are between 32 ± 2 and 37 ± 2 s and at the end of they range from 29 ± 2 to 32 ± 2 s. Interesting behavior of period can be seen on the bead No. 1, which has the same period 32 ± 2 s, and bead No. 4, which starts with 37 ± 2 s period and ends at 29 ± 2 s. Oscillations in the system with higher $[H_2SO_4]_0$ (Fig. 5e) are self-induced under $\varphi_1 = 0.0$ V with the periods 12 ± 2 s. In the time interval when the second electric potential $\varphi_2 = +0.5$ V is applied periods of all beads increase to 15 ± 2 s. The green lines in Fig. 5e mark cross sections for the space–time plots illustrated in Fig. 5f and the blue dots show locations of points at which the intensity of the green component shown in Fig. 5g is measured. Fig. 5f and g show the results obtained in the time interval [4433 s, 6233 s] in which the applied potential is $\varphi_3 = -0.5$ V. This time interval has been selected to match the lengths of time intervals of Fig. 5c and d and to show, that all beads are synchronized. Wave merging is not that clear as in Fig. 5c and d, but still can be noticed as wavy curves of green component in the space–time plots in Fig. 5e e.g. for bead No. 2. The periods shown in the given time interval are around 18 ± 2 s, which is around half of the period of the first system (Fig. 5a) with lower $[H_2SO_4]_0$. This experiment shows the importance of optimization of initial conditions of oscillatory media when we expect the global control.

The results for time evolution of another MA-CHD-BZ system with platinum wire (diameter 0.43 mm) as the working electrode and 25 beads of Dowex 50W-X8 with mesh size 50–100 used for ferroin immobilization are shown in Figs. 6 and 7. We expect to observe the effect of local control on system evolution. Unlike for case of Dowex 50W-X4 with mesh size 20–50 in Fig. 5, there is no self-initiation of oscillations. The volume of reagents is 5 ml and the initial concentrations are: $[NaBrO_3]_0 = 0.45$ M, $[MA]_0 = 0.2$ M, $[CHD]_0 = 0.2$ M, $[H_2SO_4]_0 = 0.9$ M. This system is using the same $[NaBrO_3]_0$ as in Fig. 3 because that system showed oscillations working for 13 + h. The initial concentration of H_2SO_4 is as high as in Fig. 5e–g to have shorter periods of oscillations if compared to other systems presented in this work. As in Fig. 2 the green lines mark cross sections for the space–time plots illustrated in (c) and the blue dots show locations of points at which the intensity of the green component shown in (d) was measured. The electric potentials $\varphi_1 = 0.0$ V and

$\varphi_2 = -0.5$ V in the first and second phase of experiment do not induce oscillations. The third step of electric potential $\varphi_3 = +0.5$ V induces oscillation in most of the beads. Four periods are observed, specifically 30 ± 5 s for beads No. 1–7, 10, 11, 14, 15 and 25; 50 ± 5 s for beads No. 8, 9, 12 and 22; 42 ± 5 s for beads No.13, 23 and 24; 60 ± 7 sfor beads No. 20.

The space–time plots of the green component intensity for all beads in the time interval [5500 s, 7300 s] in which the applied potential is $\varphi_4 = -0.5$ V are shown in Fig. 6c and the green component intensities observed on all beads at the blue points as functions of time in the time interval [5500 s, 7300 s] are presented in Fig. 6d. Due to a high number of analyzed beads, the intensities are placed in two-column graph. We observe, that beads oscillate mainly with two periods, the first one is 50–60 s and it applies to beads No. 2, 5, 12, 14, 21. The second one, shorter, 30 ± 4 s applies to the remaining beads. After the half of the considered time interval [5500 s, 7300 s], some oscillations get dampened and some oscillations transform into mixed mode oscillations. Dampened oscillations occur in beads No. 12 and No. 23. This feature is caused by superposition of the antiphase TW. We observed TW annihilation at the bead No. 18. Beads No. 19 and No. 20 are touching the working electrode and directly respond to the electrode potential. However, since no other bead is connected to them, signal is propagating only for a short period of time. The appearance of mixed mode oscillations in beads No. 2, and No. 10, is caused by merging of TW with shifted phase. For the bead No. 8 the longer period (L) is 23 ± 4 s and the shorter period (S) is 12 ± 4 s, therefore the MMO regime L^S is 1^1 [16]. For the bead No. 2 we observe the mix of modes with periods 50 s and 30 ± 2 s. The order of MMOs is not regular. For the bead No. 10 the long period is approx. 80 s and 2 smaller peaks have periods approx. 50 s, therefore the MMO regime L^S is 1^2. This experiment shows that one can use local control of oscillations on wave merging into MMOs and wave annihilation. It also confirms synchronisation of periods of oscillations introduced by the global control.

The endurance of MA-CHD-BZ system with ferroin loaded Dowex 50W-X8 (50–100) mesh is demonstrated in Fig. 7. The Fig. shows the same experiment as in Fig. 6 but after another 15 + h of activity and 11 electric potential steps. The space–time plots of the green component intensity for all beads in the time interval [68,760 s, 70,610 s] in which the applied potential is $\varphi_{15} = 0.0$ V are shown in Fig. 7c and the green component intensities observed on all beads at the blue points as functions of time are presented in Fig. 7d. The time interval is purposely chosen to show the evolution 19 h after the experiment was initiated to prove the beads are still oscillating and even showing interesting dynamics. The beads with number 1–6, 8, 9, 11–17 and 19 oscillate with 30 ± 4 s period. The bead No. 7 shows MMO regime with 73 ± 3 s for long period oscillation (L) and 44 ± 2 s for short period oscillations (S). The MMO sequence $(L^S)_n$, where n is number of repeating of the sequence, is 1^3, 1^5, 1^2, $(1^1)_2$, 1^2, 1^0, 1^1, $(1^0)_2$, $(1^1)_3$. The bead No 10. shows slow oscillations with periods > 600 s. The beads No. 18 and 22 show long period oscillations with period 200 s extending to approx. 270 s. The beads No. 20, 21, 23, 24, 25 show period of oscillations 70 ± 4 s. This period is approximately the double of the beads period on the left side of the working electrode, see Fig. 7a and b. The bead No. 7 shows MMOs probably because it is in the center of the left side assemblage,

see Fig. 7a and b. We think the beads No. 10, 18, 22 are located, where waves are merging, but not completely annihilating. The annihilation of waves was observed in Fig. 6d for the same bead numbers. This experiment showed us lifetime of oscillations and the influence of the local control. There is no bead, which is oscillating without the influence from potentiostat. Given time, MMOs and chaotic like oscillatory behavior is stabilized into simpler behavior, but the central bead of the assemblage kept operating in MMO regime.

Discussion and conclusions

The use of potentiostat to control MA-BZ reaction proceeding in the ferroin loaded Dowex 50W-X4 bead with mesh size 20–50 (0.569 mm average diameter) was described by Kuze et al. [29] They observed periods between 20 and 100 s, shorter periods for GO and longer periods for TW. The both types of nonlinear behavior depended on diameters of a single bead and on electric potential applied via platinum foil electrode on which the beads were located. In the following paper, the technique of switching between GO and TW inside a single bead using electric potential was developed [30]. The results of Kuze et al. were the starting point for our study on the MA-BZ systems with platinum foil electrode for global control of the system. In our experiments the periods of oscillations in ferroin loaded Dowex 50W-X4 were close to 100 s, which is equivalent for TW periods [29], specifically 75 ± 2 s and 90 ± 1 s. We think the beads must synchronize their regimes using quorum sensing [39] because GO were not observed in this set of experiments. Comparing groups of three and four ferroin loaded Dowex 50W-X4 type beads with global control, the larger group shows shorter period of oscillations when electric potential is applied. During the first few minutes of the experiment, under neutral electric potential, the group of four beads shows superposed TW for longer time than group of three beads. In the long-time experiments, the application of negative electric potential in systems of 3–9 beads with global control introduces synchronization of periods of regardless of numbers of beads in the group. The overall long-term effect of positive electric potential for systems with global control is shortening of the oscillation period. Moreover, this system produced large CO_2 bubbles for experiment longer than 5 h. Therefore, we do not think such medium is suitable for chemical computing application.

For the MA-BZ system with ferroin loaded Dowex 50W-X2 mesh 20–50 (0.644 mm average diameter) and ferroin loaded Dowex 50W-X8 mesh 16–50 (0.801 mm average diameter), for both local and global control, the system shows much lower periods of oscillations of concentrations of oxidized ferroin at the point of observation, specifically 50 ± 2 s, 30 ± 2 s, 25 ± 2 s and 20 ± 2 s than it is observed in the experiments with Dowex 50W-X4. This effect is also related to higher concentration of H_2SO_4 in the initial mixture. Despite the lengths of the periods equivalent to GO [29], we observed TW in this case. Our experiments also show, that desynchronization of the periods in beads occurs when negative electric potential is applied. The synchronization of the periods in beads occurs when neutral electric potential is applied. Oscillations can be induced inside ferroin loaded Dowex

50W-X8 with global control. However, the time difference in between periods is not controllable by negative electric potential change. Oscillations inside ferroin loaded Dowex 50W-X8 can also be induced by local control and application of negative electric potential. The periods inside ferroin loaded Dowex 50W-X8 can be influenced by local control. This feature makes Dowex 50W-X8 promising candidates in chemical computing units. On the other hand, oscillations inside ferroin loaded Dowex 50W-X2 under local control develop in time regardless of applied negative electric potential. Our systems can show oscillations for over 16 h, however at least 2 out of 8 beads used in our experiments in average were removed from their original position by CO_2 bubbles. Therefore, in our opinion the generation of CO_2 bubbles can be a problem for a practical application of this medium in chemical computing if a long time of experiment is required. On the other hand, fast oscillations are promising because they speed up of information processing. To compare with existing systems, optochemical neurocomputer [27] using BZ droplets in rubber tubings and light coupling has one of the natural pulses generator 75 s and 82 s, the rest of the droplets are susceptible to forced period of pulses. The working cycle of the optochemical neurocomputer is over an hour [27]. Another system is programmable chemical computer for pattern recognition, which works with periods 30 s to 60 s in an array of BZ droplets [3].

The working time (5–16 h) of both MA-BZ systems mentioned above can be compared with experiments performed by the other groups. Microoscillators submerged in water-in-oil emulsion can work around 6 h, and can even show Turing patterns [21]. Another system are droplets in hexadecanol oil using MA, which can work over 75 min before they get depleted [23].

We expect that a variant of BZ reaction, which does not produce CO_2 can help to increase stability of chemical computing assemblages. CHD-BZ reaction is an example of such system. We experimented on Dowex 50W-X4 (0.649 mm average diameter), with global control by potentiostat. If Br^- ions are present in the initial conditions the system was able to oscillate from the beginning for 3.5 h. The period is 20 ± 2 s during the whole experiment time if zero electric potential is applied. The application of positive electric potential dampens the oscillations. The system without addition of Br^- into initial reagents and negative electric potential that induces oscillations has a lifetime of 3.5 h. In this system oscillations do not initiate itself when no electric potential is applied. The period of oscillations of oxidized ferroin in CHD-BZ system initiated by a negative electric potential is short at the beginning (around 11 s) and gradually increases to 40–50 s before the oscillations stop. The fact, that oscillations stop can be related to cumulation of Br^- ions generated at the polarized electrode in the reaction volume. Therefore, the oscillations in CHD-BZ have much shorter lifetime if compared to MA-BZ system despite the Dowex assemblage is mechanically stable because the reaction does not produce gas bubles. This conclusion is supported by other studies. Hamik et al. [40] reported experiments with CHD-BZ droplets without addition of Br^- inside capillaries with diameter 1.1 mm and 0.75 mm, the periods of oscillation were from 8 ± 1 to 12 ± 1 s. The periods are matching periods inside our system without addition of bromide. CHD-BZ can also run inside gels, however with higher period around 83 s and lifetime

150 min or period 55 s and lifetime 210 min [25]. Shorter period, 40 s, was achieved in turbulent pattern also in gel system for 50 min [26].

According to Chang et al. [23], mixtures of MA and CHD forming MA-CHD-BZ reaction solution can solve the problem of early occurrence of CO_2 bubbles while working longer than pure CHD-BZ. Our experiments, as well as in work by Chang et al. [23] suggest the best mixture of $[MA]_0$: $[CHD]_0$ is 1:1 to avoid bubbles around the electrode and lifetime of oscillations above 12 h. We have tested two types of beads, Dowex 50W-X4 (20–50) mesh and Dowex 50W-X8 (50–100) mesh. As expected from previous experiments, Dowex 50w-×4 had only synchronization and desynchronization of beads controllable by global electric potential control. Dowex 50W-X8 on the other had shown influence of the oscillations by local control. It is also true for MA-CHD-BZ system. The working electrode sends signal directly to assemblages of beads and we can observe wave annihilation and division of TW depending on the beads layout.

Our system with the equimolar mixture of MA and CHD shows stable oscillations for over 19 h using Dowex 50W-X8 beads with mesh size 50–100. That is average diameter 0.223 mm. System by Chang et al. is stable for 12 h using 2.5 mm droplet in diameter. Both systems can perform wave merging and wave division. The advantage of our system is the electric signal input due to direct contact of beads with the working electrode of the potentiostat, which allow us to control dynamic regimes inside beads. We can also observe homogeneous oscillations in beads, but only in the smallest ones with diameter lower than approximately 0.23 mm. For beads with bigger diameters, spatiotemporal waves inside beads are still observable.

In our opinion Dowex 50W-X8 beads with mesh size 50–100 is a promising candidate for chemical computing assemblage working for a day. Our future work will be focused on shortening electric signal impulses and the bead lattice architecture to perform simple chemical computing tasks.

Simulations of the time evolution of the discussed systems based on kinetic equations present a significant theoretical challenge and go far beyond simple models based on a few variables. We plan to present such description in the following papers.

Supplementary Information The online version contains supplementary material available at https://doi.org/10.1007/s11144-022-02171-4.

Acknowledgements This publication is part of a project that has received funding from the European Union's Horizon 2020 research and innovation programme under the Marie Skłodowska-Curie Grant Agreement No. 847413. Scientific work published as part of an international co-financed project founded from the programme of the Minister of Science and Higher Education entitled "PMW" in the years 2020–2024; Agreement No. 5005/H2020-MSCA-COFUND/2019/2.

Declarations

Conflict of interest There are no conflict to declare.

References

1. Gupta U, Kim YG, Lee S, Tse J, Lee H-HS, Wei G-Y, Brooks D, Wu C-J (2021) HPCA2021. http://arXiv.org/2011.02839
2. Adamatzky A (2019) Philos Trans R Soc B 374:20180372–20180418. https://doi.org/10.1098/rstb.2018.0372
3. Parrilla-Gutierrez JM, Sharma A, Tsuda S, Cooper GJT, Aragon-Camarasa G, Donkers K, Cronin L (2020) Nat Commun 11:1442. https://doi.org/10.1038/s41467-020-15190-3
4. Gorecki J, Bose A (2020) Front Chem 09:580703–580711. https://doi.org/10.3389/fchem.2020.580703
5. Bian J, Cao Z, Zhou P (2021) Appl Phys Rev 8:041313. https://doi.org/10.1063/5.0067352
6. Tyowua AT, Ahor F, Yiase SG, Binks BP (2020) SN Appl Sci 2:345. https://doi.org/10.1007/s42452-020-2174-9
7. Markran H (2012) Sci Am 306(6):50–55. https://doi.org/10.1038/scientificamerican0612-50
8. Balasurbramanian V (2021) PNAS 118(32):e2107022118. https://doi.org/10.1073/pnas.2107022118
9. Katz E (ed) (2021) DNA- and RNA-based computing systems, 1st edn. Wiley, Weinheim
10. Muzika F, Schreiber I (2013) J Chem Phys 139:164108. https://doi.org/10.1063/1.4825379
11. Muzika F, Schreiber I (2014) RSC Adv 4(99):56165–56173. https://doi.org/10.1039/C4RA08859J
12. Muzika F, Schreiberová L, Schreiber I (2016) Reac Kinet Mech Cat 118:99–114. https://doi.org/10.1007/s11144-016-1004-y
13. Adamtazky A (2021) Biosystems 208:104480. https://doi.org/10.1016/j.biosystems.2021.104480
14. Belousov BP (1959) Med. Publ., Moscow
15. Zhabotinsky AM (1964) Biofizika 9:306–311
16. Freirich AG, Yengi D (2021) RSC Adv 11:16435–16444. https://doi.org/10.1039/d1ra01734a
17. Papineau D, Yin J, Devine KG, Liu D, Zhenbing S (2021) Minerals 11(10):1060. https://doi.org/10.3390/min11101060
18. Geher-Herczegh T, Wang Z, Masuda T, Yoshida R, Vasudevan N, Hayashi Y (2021) Macromolecules 54(13):6430–6439. https://doi.org/10.1021/acs.macromol.1c00402
19. Safonov DA, Vanag KV (2021) Chaos 31(6):063134. https://doi.org/10.1063/5.0046051
20. Suematsu NJ, Nakata S (2021) Materials 14(20):6177. https://doi.org/10.3390/ma14206177
21. Mallphanov IL, Vanag KV (2021) Phys Chem Chem Phys 23:9130–9138. https://doi.org/10.1039/D1CP00758K
22. Gorecki J, Gizynski K, Guzowski J, Gorecka JN, Garstecki P, Gruenert G, Dittrich P (2015) Philos Trans R Soc A 373:20140219. https://doi.org/10.1098/rsta.2014.0219
23. Chang MK, de Planque MNR, Zauner KP (2018) Sci Rep 8:12656. https://doi.org/10.1038/s41598-018-30819-6
24. Gizynski K, Gorecki J (2017) Phys Chem Chem Phys 19(9):6519–6531. https://doi.org/10.1039/C6CP07492H
25. Otsuka Y, Maeda S (2020) Chem Lett 49:863–866. https://doi.org/10.1246/cl.200219
26. Anupong S, Schreiber I, Kheowan O-U (2021) Phys Chem Chem Phys 22:28213–28221. https://doi.org/10.1039/d0cp04112b
27. Proskurkin IS, Smelov PS, Vanag KV (2020) Phys Chem Chem Phys 22:19359–19367. https://doi.org/10.1039/d0cp01858a
28. Hwang I, Mukhopadhyay RD, Dhasaiyan P, Choi S, Kim S-YK, Young HK, Kangkyun B, Kim K (2020) Nat Chem 12:808–813. https://doi.org/10.1038/s41557-020-0516-2
29. Kuze M, Horisaka M, Suematsu NJ, Amemiya T, Steinbock O, Nakata S (2019) J Phys Chem A 123:4853–4857. https://doi.org/10.1021/acs.jpca.9b02636
30. Kuze M, Horisaka M, Suematsu NJ, Amemiya T, Steinbock O, Nakata S (2021) J Phys Chem B 25(14):3638–3643. https://doi.org/10.1021/acs.jpcb.0c11019
31. Aihara R, Yoshikawa K (2001) J Phys Chem A 105:8445–8448. https://doi.org/10.1021/jp010908r
32. Zhao J, Chen Y, Wang J (2005) J Chem Phys 122:114514–114517. https://doi.org/10.1063/1.1877112

33. Szalai I, Kurin-Csörgei K, Epstein IR, Orbán M (2003) J Phys Chem A 107:10074–10081. https://doi.org/10.1021/jp0360523
34. Gorecki J (2020) Entropy 22:313. https://doi.org/10.3390/e22030313
35. Gorecki J, Gorecka JN, Adamatzky A (2014) Phys Rev E 89:42910–43010. https://doi.org/10.1103/PhysRevE.89.042910
36. Bose A, Gorecki J (2021) Int J Unconv Comput 16:1–18
37. Kuze M, Kitahata H, Steinbock O, Nakata S (2018) J Phys Chem A 122(8):1967–2197. https://doi.org/10.1021/acs.jpca.7b12210
38. Image J. https://imagej.nih.gov/ij/. Accessed 4 Nov 2021
39. Taylor AF et al (2015) Phys Chem Chem Phys 17:20047. https://doi.org/10.1039/c5cp01964h
40. Hamik TC, Manz N, Steinbock O (2001) J Phys Chem A 105:6144–6153. https://doi.org/10.1021/jp010270j